



OPEN ACCESS

EDITED BY

Suvaradhan Kanchi,
Sambhram Institute of Technology,
India

REVIEWED BY

Muhammad Kashif Shahid,
Chungnam National University, South
Korea
Ishaq Ahmad,
The University of Hong Kong, Hong
Kong SAR, China

*CORRESPONDENCE

Junsheng Guo,
19759922@163.com

SPECIALTY SECTION

This article was submitted to Green and
Sustainable Chemistry,
a section of the journal
Frontiers in Chemistry

RECEIVED 15 July 2022

ACCEPTED 12 September 2022

PUBLISHED 27 September 2022

CITATION

Wang H, Xing Z, Sun Y, Jing Y, Zhang J,
Li X, Zhang H, Shakoor A and Guo J
(2022), UV-irradiating synthesis of
cyclodextrin–silver nanocluster
decorated TiO₂ nanoparticles for
photocatalytic enhanced anticancer
effect on HeLa cancer cells.
Front. Chem. 10:995261.
doi: 10.3389/fchem.2022.995261

COPYRIGHT

© 2022 Wang, Xing, Sun, Jing, Zhang, Li,
Zhang, Shakoor and Guo. This is an
open-access article distributed under
the terms of the [Creative Commons
Attribution License \(CC BY\)](https://creativecommons.org/licenses/by/4.0/). The use,
distribution or reproduction in other
forums is permitted, provided the
original author(s) and the copyright
owner(s) are credited and that the
original publication in this journal is
cited, in accordance with accepted
academic practice. No use, distribution
or reproduction is permitted which does
not comply with these terms.

UV-irradiating synthesis of cyclodextrin–silver nanocluster decorated TiO₂ nanoparticles for photocatalytic enhanced anticancer effect on HeLa cancer cells

Hongying Wang^{1,2,3}, Ze Xing⁴, Yan Sun², Yingjie Jing², Jian Zhang⁵, Xinyao Li⁶, Hailiang Zhang⁷, Adnan Shakoor⁸ and Junsheng Guo^{5*}

¹Thoracic Trauma and Oncology Institute, Chifeng University, Chifeng, China, ²Department of Respiratory and Critical Care Medicine, Chifeng University Affiliated Hospital, Chifeng, China, ³Department of Respiratory and Critical Care Medicine, The Affiliated Nanhua Hospital, Hengyang Medical School, University of South China, Hengyang, China, ⁴Department of Oncology Medicine, Inner Mongolia Medical University Affiliated Hospital, Hohhot, China, ⁵Department of Urology, Chifeng University Affiliated Hospital, Chifeng, China, ⁶School of Stomatology, Chifeng University, Chifeng, China, ⁷Guangdong Huace Biomedical Research Center, Guangzhou, China, ⁸Department of Control and Instrumentation Engineering, King Fahd University of Petroleum and Minerals, Dhahran, Saudi Arabia

Titanium dioxide (TiO₂) has emerged as a viable choice for several biological and environmental applications because of its high efficiency, cheap cost, and high photostability. In pursuit of this purpose, the research of its many forms has been influenced by these unique aspects. The development of novel TiO₂-based hybrid materials with enhanced photocatalytically induced anticancer activity has gained tremendous attention. Here, we have developed a novel photocatalytic material (TiO₂-Ag NPs@-CD) by decorating ultrasmall silver nanoparticles (Ag NPs) with per-6-thio-β-cyclodextrin (SH-β-CD) on TiO₂ NPs. TiO₂-Ag NPs@-CD were characterized by employing various characterization techniques and evaluated for their anticancer activity against HeLa cancer cells using an MTT assay. The biocompatibility of the designed nanoparticles was determined on two normal cell lines, namely, 3T3 and human mesenchymal stem cells (hMSCs). The results show that the TiO₂-Ag NPs@-CD induced superior cytotoxic effects on HeLa cancer cells at a concentration of 64 μg/ml. Live-dead staining and oxidative stress investigations demonstrated that cell membrane disintegration and ROS-induced oxidative stress generated by TiO₂-Ag NPs@-CD inside HeLa cancer cells are the contributing factors to their exceptional anti-cancer performance. Moreover, TiO₂-Ag NPs@-CD exhibited good biocompatibility with 3T3 and hMSCs. These results indicated that the combination of all three components—a silver core, SH-β-CD ligands, and TiO₂ nanoparticles—produced a synergistic anticancer effect. Hence, the TiO₂-Ag NPs@-CD is a promising material that can be employed for different biological applications.

KEYWORDS

TiO₂, cyclodextrin-silver, photocatalytic, anticancer, HeLa, cervical

Introduction

Over the past few decades, cancer has become the second-leading cause of death globally (Siegel et al., 2020). In terms of morbidity and prevalence, cervical cancer (CCA) is a disease that affects women and is ranked fourth globally (Canfell et al., 2020). Although human papillomavirus vaccination, new chemotherapeutic drugs, and other therapeutic techniques provide efficient control and treatment of cervical cancer, metastatic CCA is an acute or chronic cancer that urgently requires novel anticancer drugs and therapeutic strategies for treatment (Brisson et al., 2020; Cohen et al., 2020).

As nanotechnology has advanced, nanomaterials have been considered for anticancer applications (Khan et al., 2018a, 2018b, 2021; Khan and Lee, 2020; Lu et al., 2021). Numerous studies have been conducted on photocatalysts that use distinct portions of the solar spectrum. The electrons and hole pairs, created by the absorption of visible light on photocatalytic nanomaterials, can independently react with water and oxygen. Once reacted with oxygen and water, they make a variety of reactive oxygen species (ROS) (Yang et al., 2022). The cell membrane may become oxidatively damaged as a result of these ROS interactions with polysaccharides, lipids, proteins, and other organelles of the cell (Wang et al., 2017; Khan et al., 2020b; Sher et al., 2021). At a pH of 7, the oxidation of water at the hole side results in a potential for the generation of ROS that is 1.11–1.9 eV compared to the standard hydrogen electrode [12]. As a result, the bandgap of nanomaterials is an essential component that plays a role in the formation of ROS *via* photocatalysis (Liu et al., 2016; Khan et al., 2019a, Khan et al., 2019b). Moreover, while working as photocatalysts, numerous nanomaterials produce anticancer phenomena *via* the production of ROS (Hariharan et al., 2020). Notably, photocatalysis is essential and has excellent potential in killing cancer cells effectively (Zhao et al., 2021). The development of anticancer nanomaterials with specific properties, such as low toxicity, high anticancer activity, and photo-reactivity, remains a formidable challenge.

Titanium dioxide (TiO₂), a conventional semiconductor material, is a good choice for anticancer applications owing to its low toxicity, excellent photostability, cheap cost and strong photocatalytic performance (Tada et al., 2009; Schneider et al., 2014; Zhu et al., 2018). UV light would cause the formation of electron-hole pairs when TiO₂ was utilized as a photocatalyst. The electron-hole pairs may combine with water or oxygen to generate reactive oxygen species, such as superoxide radicals (O₂^{•-}) and hydroxyl radicals (•OH) (Liu et al., 2010). These highly reactive

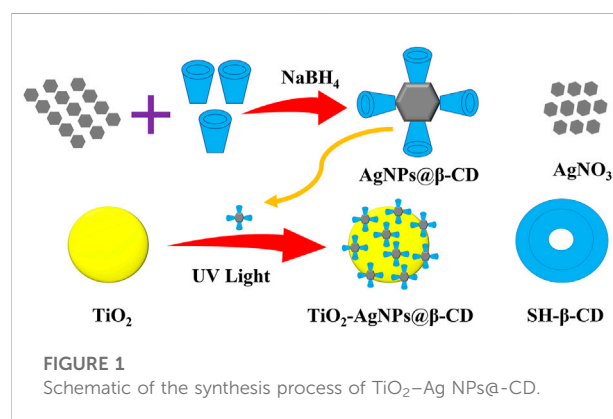
species induce phototoxicity and cause cancer cell death. Despite TiO₂'s photocatalytic potential, its rapid electron and hole recombination would limit its efficiency. To reduce this effect and improve the photocatalytic efficacy of TiO₂, noble metal nanoparticles (NPs) such as Ag, Au, etc., might be utilized (Liu et al., 2010, 2016b).

To address the aforementioned grim issues, we have developed a novel photocatalyst by decorating ultrasmall silver nanoparticles (Ag NPs) with per-6-thio-β-cyclodextrin (SH-β-CD) on TiO₂ NPs (Figure 1). Particularly, SH-β-CD can be utilized to synthesize ultrasmall Ag NPs (Ag NPs@β-CD) (Liu et al., 2000; Negishi et al., 2005), and it can also improve the interaction between Ag NPs and TiO₂ NPs (Zhang et al., 2012; Li et al., 2015). Hence, an important element of our strategy is the utilization of SH-β-CD, which promotes the connection between Ag NPs and TiO₂ NPs, resulting in the development of an effective photocatalyst. Moreover, through the host-guest interaction, the unique cavity in the toroidal structure of SH-β-CD makes the silver core further reachable to the organic moieties of the cells (Zhang et al., 2010; Chalasani and Vasudevan, 2013; Devi and Mandal, 2013; Yang et al., 2014; Alsbaiee et al., 2016; Wang et al., 2016). The combination of all three components—SH-β-CD ligands, a silver core, and TiO₂ nanoparticles—produced a synergistic anticancer effect that resulted in a significant enhancement of photocatalytic-induced cytotoxicity of the material.

Materials and methods

Chemicals

Chemicals were commercially available and used as received. NaOH ≥99% were acquired from Merck. AgNO₃ ≥99.0%,



NaBH₄ ≥98%, TiO₂, Calcein-AM, and propidium iodide were purchased from Sigma-Aldrich. SH-β-CD was purchased from Shandong Binzhou Zhiyuan Bio-Technology CO., Ltd. (China). HeLa, hMSCs, and 3T3 cell lines were bought from ATCC (Manassas, USA). CellROX™ Green and dialysis tube (MWCO 6000–8,000 Da) were purchased from ThermoFisher.

Synthesis of Ag NPs@-CD

The Ag NPs@-CD was synthesized following the method reported previously with slight modifications (Zhu et al., 2018). In detail, 10 mM SH-β-CD and 40 mM AgNO₃ solutions were made using 0.1 M NaOH and ultrapure water, respectively. For the development of Ag NPs@β-CD, 250 μL of AgNO₃ and 286 μL of SH-β-CD were mixed in 9.2 ml of ultrapure water in a glass bottle. Then, 40 μL of a 1 M solution of NaOH was included in the reaction mixture and then mixed for 2 hours at 25°C. Then, 8.6 mg of pure NaBH₄ was added to 2 ml of 0.1 M NaOH solution to prepare the NaBH₄ solution. Then, 200 μL NaBH₄ was poured into the reaction mixture and mixed for 6 hours at 25°C to obtain Ag NPs@β-CD. Then by utilizing a dialysis tube (MWCO 6000–8,000 Da), the synthesized Ag NPs@β-CD were purified by dialysis for 24 h.

Synthesis of TiO₂-Ag NPs@-CD

The TiO₂-Ag NPs@-CD was synthesized following the method reported previously with slight modifications (Zhu et al., 2018) (Figure 1). 10 ml of Ag NPs@β-CD solution at 0.4 mM concentration was mixed with 10 mg of TiO₂ powder followed by 40 min of stirring under UV irradiation. The resultant materials were then centrifuged and rinsed three times with pure water to get TiO₂-Ag NPs@β-CD.

Characterization

Powder X-ray diffraction spectroscopy (XRD) was utilized to determine the phase purity and crystalline nature of the TiO₂-Ag NPs@-CD. For this purpose, Bruker D₂ PHASER with LYNXEYE XE-T detector (Haidian, Beijing, China) was used at a wavelength (λ) of 0.154 nm. The XRD spectra were acquired in the 2θ range of 5°–60°. An energy-dispersive X-ray (EDX) spectroscopy equipment (Thermo Fisher Scientific Ultradry (Madison, WI, USA) linked to a scanning electron microscope was used to analyze the chemical composition of the generated TiO₂-Ag NPs@-CD. A Tecnai F12 microscope (FEI/Philips Tecnai 12 BioTWIN, Baltimore, MD, USA) was utilized to obtain TEM images of the TiO₂-Ag NPs@-CD at 200 kV acceleration voltage. Before being placed on a carbon-coated copper grid for TEM examination, the samples were mixed in methanol. Then the

mixture was sonicated at 25–30°C. The copper grid was dried 5–10 min after draining the excess solution.

Cell line and culture

HeLa, hMSCs, and 3T3 cell lines were bought from ATCC (Manassas, USA). Cells were grown in DMEM supplemented with 10% FBS (v/v), 100 U/mL penicillin, and 100 μg/ml streptomycin at 37°C in a humidified incubator with 5% CO₂. Cells were subcultured once their confluency reached 80 percent. For tests, cells in the logarithmic growth phase were utilized.

Cell viability analysis

MTT assay was used to analyze cell viability with slight modifications (Khan et al., 2020a; Xu et al., 2020). Briefly, HeLa cells were incubated for 2 h at 37°C in 96-well plates with 100 μL of samples at different concentrations of 0.5, 1.0, 2.0, 4.0, 8.0, 16, 32, and 64 μg/ml. Then they were irradiated with a GGZ-300W high-pressure Hg lamp (E_{max} = 365 nm) at room temperature. A UV pass filter was used to obtain a light wavelength between 300 and 400 nm. The light intensity at the liquid surface was measured by a VLX-3W radiometer-photometer (USA). The incident light intensity was 3.7 mW/cm² (Zhang and Sun, 2004). Control was prepared without treatment. Each well received 10 μL of MTT (5 mg/ml) and was incubated for 4 h. To dissolve the crystal formazan dye, 150 μL of DMSO was added to the medium, and optical density was measured at 540 nm using a Microplate Reader. The cell viability was calculated utilizing the following formula.

$$\text{Cell viability (\%)} = (\text{OD}_s/\text{OD}_c) \times 100$$

Where OD_s and OD_c are optical densities of sample and control, respectively.

Live-dead staining assay

A live-dead staining assay was conducted following the protocol reported previously in (Xu et al., 2020). In detail, after 24 h of the incubation of HeLa cells with 100 μL of the TiO₂-Ag NPs@-CD at 64 μg/ml, the cells were rinsed with PBS and stained with a Live-dead cell viability kit by following the manufacturer's instructions to determine the cell viability. In summary, cells were treated with 2 and 4.5 μM of calcein-AM and propidium iodide (PI) staining solution, respectively. Following this, cells were incubated for 30 min at 37°C. The Live-dead kit determines cell viability based on the integrity of the cell membrane. CLSM (confocal laser scanning microscope) was used to observe live and dead cells, with excitation wavelengths of 490 and 535 nm for Calcein-AM and PI and emission wavelengths of 515 and 617 nm for Calcein-AM and PI, respectively. We only investigated TiO₂-Ag NPs@-CD for the

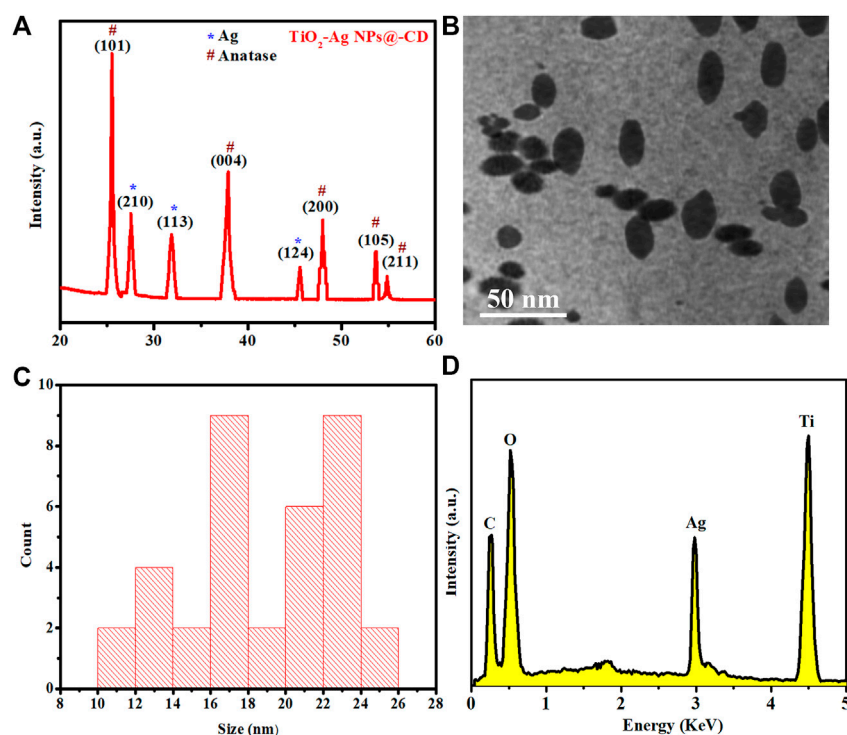


FIGURE 2
(A) XRD, (B) TEM, (C) size distribution, and (D) EDX of synthesized TiO_2 -Ag NPs@-CD.

Live-dead staining experiment because they showed good cytotoxic effects on HeLa cancer cells.

ROS and oxidative stress measurement

As previously reported (Lu et al., 2021), CellROX™ Green (C10444, ThermoFisher) was used to investigate the death of HeLa cancer cells due to ROS generation. HeLa cancer cells were treated with 100 μL of TiO_2 -Ag NPs@-CD at a concentration of 64 $\mu\text{g}/\text{ml}$ and incubated for 24 h at 37°C. The HeLa cancer cells were subsequently treated for an additional 30 min at 37°C with CellROX™ Green (5 μM). CLSM was then utilized to obtain pictures with excitation wavelengths of 485 nm and emission wavelengths of 520 nm. ROS generation in TiO_2 -Ag NPs@-CD treated cells was compared to untreated cells (negative control) and those treated with 1 mM H_2O_2 (positive control).

Biocompatibility analysis

The MTT technique was employed to evaluate the biocompatibility of Ag NPs@-CD and TiO_2 -Ag NPs@-CD with hMSCs and 3T3 cells in terms of cell viability (%). The same protocol is repeated as described in *Cell line and culture*

Section and *Cell viability analysis* Section. The 100 μL of both samples at the concentration of 64 $\mu\text{g}/\text{ml}$ were used as a treatment for both cell lines.

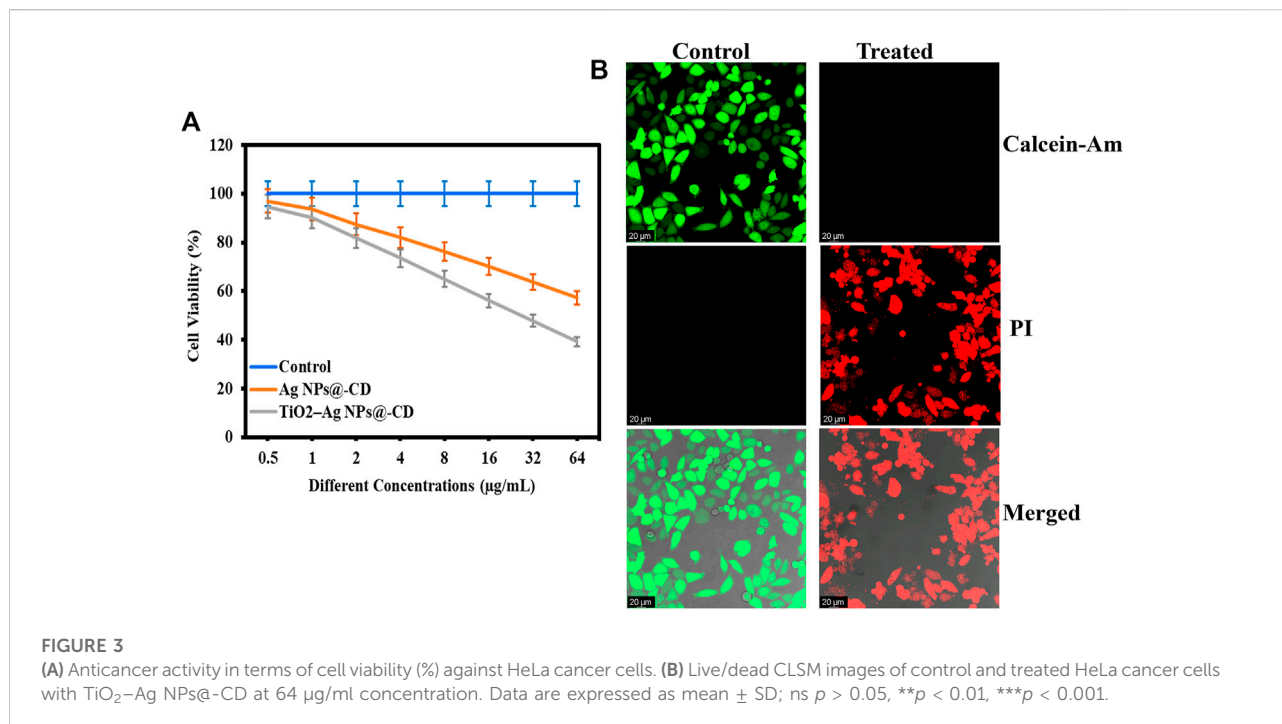
Statistics analysis

All biological tests were conducted in triplicate, and data are reported as the mean \pm standard deviation. In addition, we utilized one-way and two-way ANOVA to determine the significant level of 0.05.

Results and discussion

Characterization

The TiO_2 -Ag NPs@-CD were characterized for their crystallinity using XRD. Figure 2A shows the XRD spectra. XRD pattern reveals the peaks indexed to (101), (004), (200), (105), and (211) planes of anatase TiO_2 at 2θ angles of 25.50°, 37.92°, 48.01°, 53.71°, and 54.88°, respectively. The XRD pattern of TiO_2 is closely matched with JCPDS 21-1272 (Abdelsalam et al., 2020). No peaks associated with the rutile phase of TiO_2 were observed. In addition, the XRD



pattern also demonstrated the existence of other peaks indexed to (210), (113), and (214) crystal planes of Ag at 2θ angles of 27.51° , 31.87° , and 45.57° , respectively (Karthik et al., 2014). The peak's intensity and their sharpness indicate that the TiO₂-Ag NPs@-CD are highly crystalline in nature. Figure 2B shows the TEM image, which demonstrates that the TiO₂-Ag NPs@-CD have spherical and oval morphology with uniform dispersion. No agglomeration was observed. Figure 2C shows the histogram for the size distribution determined from TEM. The histogram shows that they have an average size of 18.98 ± 4.1 . The compositional analysis of TiO₂-Ag NPs@-CD was performed using EDX. Figure 2D depicts the EDX spectrum. EDX pattern exhibits that the synthesized material is mainly composed of silver, titanium, and oxygen. Moreover, carbon peak is also evident in the EDX spectrum, which can be attributed to the CD. Abdelsalam et al. also reported similar EDX pattern results for Ag-doped TiO₂ NPs (Abdelsalam et al., 2020).

Cell viability analysis

The anticancer activity of Ag NPs@-CD and TiO₂-Ag NPs@-CD against HeLa cancer cells was determined using an MTT assay. Figure 3A shows the results in terms of cell viability (%). Both samples presented concentration-dependent anticancer activity against HeLa cancer cells. The results further show that the least cell

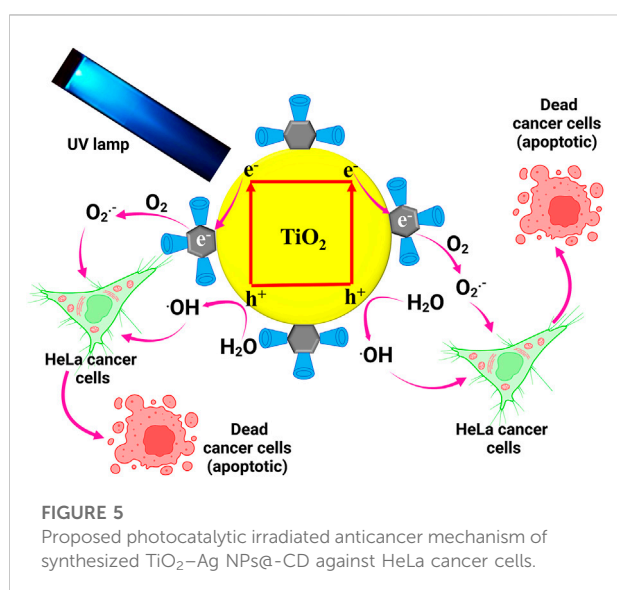
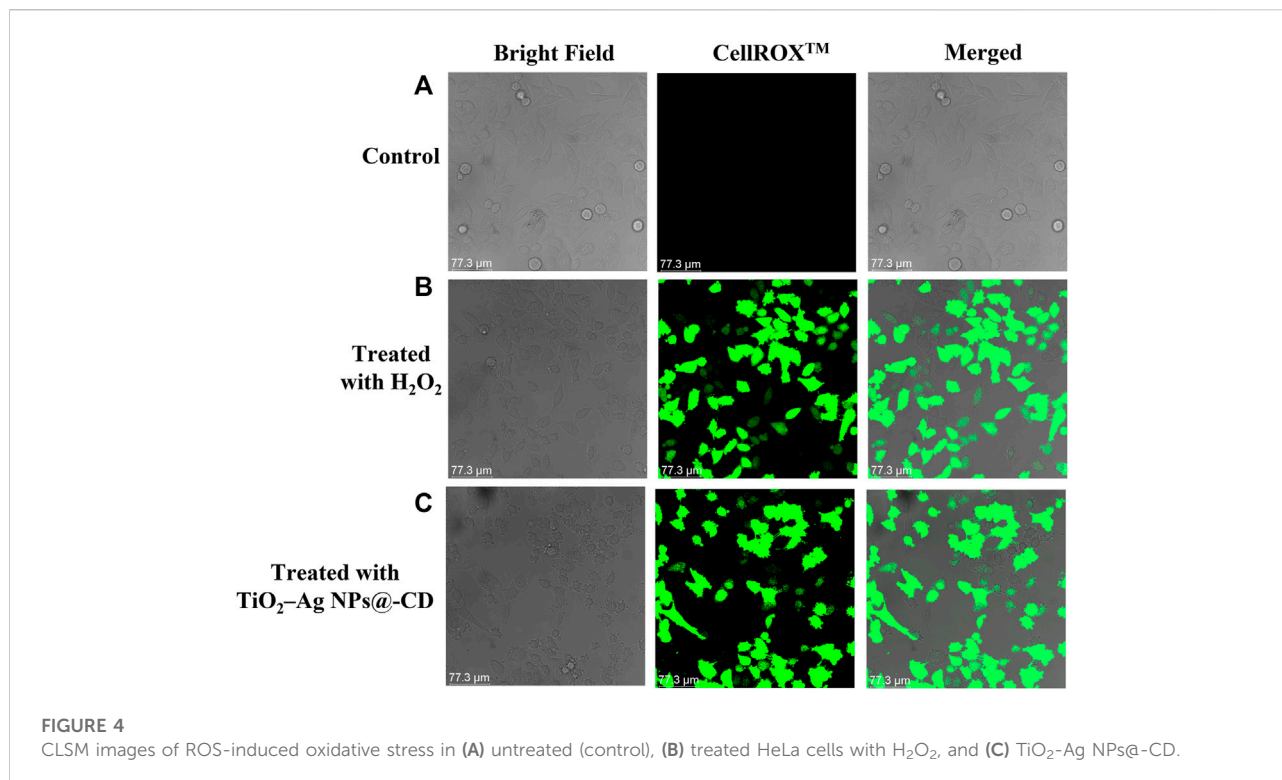
viability (%) of HeLa cells was manifested with TiO₂-Ag NPs@-CD compared to Ag NPs@-CD at all tested concentrations.

Live/dead staining analysis

A Live/dead staining assay was further performed after treatment of HeLa cancer cells with TiO₂-Ag NPs@-CD at 64 µg/ml to affirm the inhibition of cell proliferation. The live cells were stained with Calcein-Am (Green), and the dead were labeled with PI (Red). The results are presented in Figure 3B. In contrast, to control, HeLa cells treated with TiO₂-Ag NPs@-CD emitted stronger red fluorescence, indicating that their cell membrane had been damaged. Furthermore, treated HeLa cells displayed abnormal shape and aggregation, indicating the presence of a more significant number of apoptotic cells. As a result of these observations, it is conceivable that the anticancer activity of TiO₂-Ag NPs@-CD is attributable to their ability to damage the cell membrane of HeLa cancer cells.

ROS and oxidative stress analysis

We have further investigated the performance of ROS-induced oxidative stress in destroying HeLa cancer cells. It is well established that nanomaterials induced apoptotic cell



death in neoplastic cells *via* the oxidative stress triggered by the generation of ROS. ROS generate oxidative stress by their intercalation with different organelles inside the cells. Therefore, ROS-induced oxidative stress was by employing a CellROX™ Green staining kit. The HeLa cancer cells were treated with 100 μ L of TiO₂-Ag NPs@-CD (64 μ g/ml concentration) and H₂O₂ (positive control) and further

stained with CellROX™ Green. After incubation, the images were acquired using CLSM. As shown in Figures 4A–C, CLSM images demonstrate that untreated HeLa carcinoma cells do not produce intracellular ROS. However, HeLa cancer cells treated with TiO₂-Ag NPs@-CD and H₂O₂ exhibited adequate and significant levels of green fluorescence. A similar observation was also reported by Hariharan et al. (Hariharan et al., 2020). These results imply that the ROS-induced oxidative stress caused by TiO₂-Ag NPs@-CD within HeLa cancer cells is also a contributing factor to their extraordinary anti-cancer performance.

Anticancer mechanism

Based on the results from the experiments, we proposed the photocatalytic irradiated anticancer mechanism of synthesized TiO₂-Ag NPs@-CD against HeLa cancer cells, as shown in Figure 5. When exposed to UV light, the excited electrons move to the Ag core, forming a new redox center. These electrons then combine with oxygen at the Ag core, producing reactive O₂^{•-}. Furthermore, the presence of SH-CD on the Ag core's surface may efficiently trap cancer cells through a host-guest interaction. Cancer cells begin to perish when they diffuse to active locations due to the reactive O₂^{•-}. The holes, on the other hand, may react

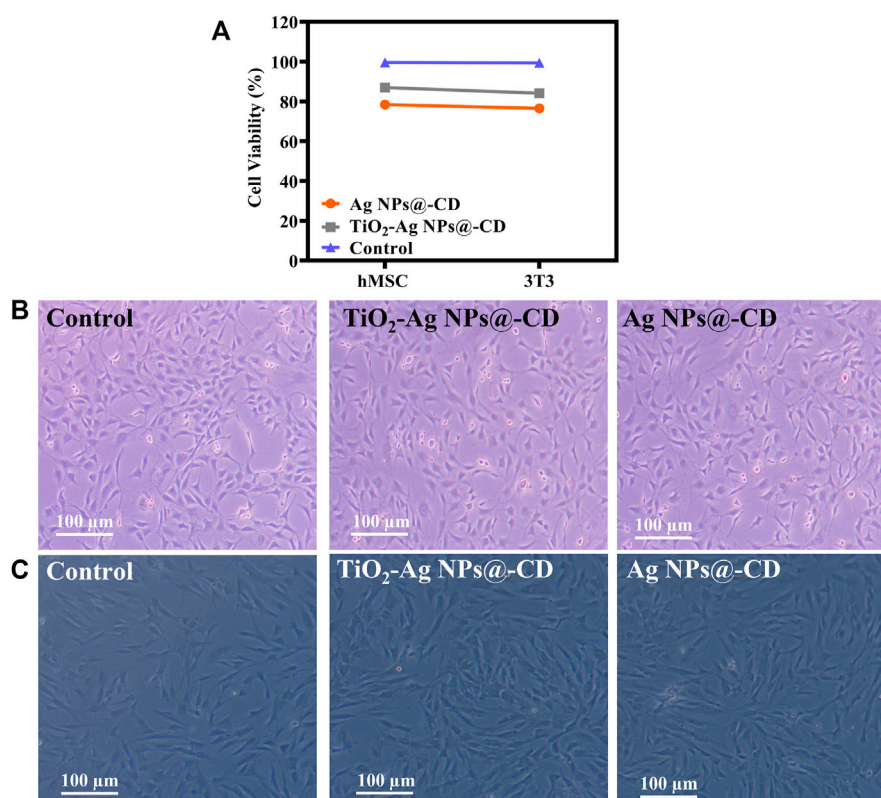


FIGURE 6

(A) Biocompatibility of Ag NPs@-CD and TiO₂-Ag NPs@-CD with hMSC and 3T3 cells. Inverted micrographs of (B) 3T3 and (C) hMSC. Data are expressed as mean ± SD; ****p* < 0.001, *****p* < 0.0001.

with water to produce $\bullet\text{OH}$ radicals, which would also increase the induction of toxicity in HeLa cancer cells, leading to apoptosis. Taken together, the improved photocatalytic irradiated anticancer activity of the TiO₂-Ag NPs@-CD may be attributed to the synergy between all three components, namely the Ag core SH-CD ligands and TiO₂ NPs. A similar enhanced photocatalytic performance was also reported by (Zhu et al., 2018).

Biocompatibility investigations

Biocompatibility of Ag NPs@-CD and TiO₂-Ag NPs@-CD with hMSC and 3T3 cells was determined in terms of cell viability (%). Figure 6A shows the cell viability (%) results. The findings demonstrate that TiO₂-Ag NPs@-CD exhibited high biocompatibility with hMSC and 3T3 cells. However, it seems that hMSC cells are more biocompatible. While Ag NPs@-CD exhibited lower biocompatibility with hMSC and 3T3 cells than TiO₂-Ag NPs@-CD.

Using an inverted microscope, we next examined the morphologic vicissitudes in hMSC and 3T3 cells treated with TiO₂-Ag NPs@-CD and Ag NPs@-CD at a concentration of 64 μg/ml. Figures 6B,C illustrate the inverted micrographs of 3T3 and hMSC cells, respectively. After treatment with TiO₂-Ag NPs@-CD, the morphology of hMSC and 3T3 cells was comparable to that of the control group (untreated cells). However, Ag NPs@-CD was marginally toxic to hMSC and 3T3 cells as there was a slight change in the shape and size of the cells. The findings of inverted microscopy and cell viability were found to be comparable. As a result, the improved biocompatibility may be attributed to TiO₂ NPs contained in TiO₂-Ag NPs@-CD.

Conclusion

In summary, we successfully synthesized novel TiO₂-Ag NPs@-CD and explored their anticancer effect on HeLa cancer cells *in vitro*. We have determined that cell membrane disintegration and ROS-induced oxidative stress generated by TiO₂-Ag NPs@-CD inside HeLa cancer cells are

the contributing factors to their exceptional anti-cancer performance. TiO₂-Ag NPs@-CD is highly biocompatible with both hMSC and 3T3 cells, which indicates their importance in being employed in pharmacological and clinical applications. Future research is required to assess the dose-dependent *in vivo* cytotoxic and biocompatibility. In addition, this work will provide the opportunity for the continued development of biocompatible materials with improved biological properties.

Data availability statement

The raw data supporting the conclusions of this article will be made available by the authors, without undue reservation.

Author contributions

Conceptualization, HW, ZX, YS, YJ, and JZ; methodology, HW, ZX, YS, YJ, and JZ; software, HW, ZX, YS, YJ, and JZ; validation, HW, ZX, YS, YJ, and JZ; formal analysis, HW, ZX, YS, YJ, and JZ; investigation, HW, ZX, YS, YJ, and JZ; resources, XL, HZ, AS, and JG; data curation, XL, HZ, AS, and JG; writing—original draft preparation, HW, ZX, YS, YJ, and JZ; writing—review and editing, XL, HZ, AS, and JG; visualization, XL, HZ, AS, and JG; supervision, HW and JG; project administration, JG; funding acquisition, HW and JG. All authors have read and agreed to the published version of the manuscript.

References

- Abdelsalam, E. M., Mohamed, Y. M. A., Abdelkhalik, S., el Nazer, H. A., and Attia, Y. A. (2020). Photocatalytic oxidation of nitrogen oxides (NO_x) using Ag- and Pt-doped TiO₂ nanoparticles under visible light irradiation. *Environ. Sci. Pollut. Res.* 27, 35828–35836. doi:10.1007/s11356-020-09649-5
- Alsaiee, A., Smith, B. J., Xiao, L., Ling, Y., Helbling, D. E., and Dichtel, W. R. (2016). Rapid removal of organic micropollutants from water by a porous β-cyclodextrin polymer. *nature* 529, 190–194. doi:10.1038/nature16185
- Brisson, M., Kim, J. J., Canfell, K., Drolet, M., Gingras, G., Burger, E. A., et al. (2020). Impact of HPV vaccination and cervical screening on cervical cancer elimination: A comparative modelling analysis in 78 low-income and lower-middle-income countries. *Lancet* 395, 575–590. doi:10.1016/s0140-6736(20)30068-4
- Canfell, K., Kim, J. J., Brisson, M., Keane, A., Simms, K. T., Caruana, M., et al. (2020). Mortality impact of achieving WHO cervical cancer elimination targets: A comparative modelling analysis in 78 low-income and lower-middle-income countries. *Lancet* 395, 591–603. doi:10.1016/s0140-6736(20)30157-4
- Chalasani, R., and Vasudevan, S. (2013). Cyclodextrin-functionalized Fe₃O₄@TiO₂: Reusable, magnetic nanoparticles for photocatalytic degradation of endocrine-disrupting chemicals in water supplies. *ACS Nano* 7, 4093–4104. doi:10.1021/nn400287k
- Cohen, A. C., Roane, B. M., and Leath, C. A. (2020). Novel therapeutics for recurrent cervical cancer: Moving towards personalized therapy. *Drugs* 80, 217–227. doi:10.1007/s40265-019-01249-z
- Devi, L. B., and Mandal, A. B. (2013). Self-assembly of Ag nanoparticles using hydroxypropyl cyclodextrin: Synthesis, characterisation and application for the catalytic reduction of p-nitrophenol. *RSC Adv.* 3, 5238–5253. doi:10.1039/c3ra23014g
- Harihara, D., Thangamuniyandi, P., Jegatha Christy, A., Vasantharaja, R., Selvakumar, P., Sagadevan, S., et al. (2020). Enhanced photocatalysis and anticancer activity of green hydrothermal synthesized Ag@TiO₂ nanoparticles. *J. Photochem. Photobiol. B Biol.* 202, 111636. doi:10.1016/j.jphotobiol.2019.111636
- Karthik, L., Kumar, G., Kirthi, A. V., Rahuman, A. A., and Bhaskara Rao, K. V. (2014). Streptomyces sp. LK3 mediated synthesis of silver nanoparticles and its biomedical application. *Bioprocess Biosyst. Eng.* 37, 261–267. doi:10.1007/s00449-013-0994-3
- Khan, S. A., Arshad, Z., Shahid, S., Arshad, I., Rizwan, K., Sher, M., et al. (2019a). Synthesis of TiO₂/graphene oxide nanocomposites for their enhanced photocatalytic activity against methylene blue dye and ciprofloxacin. *Compos. Part B Eng.* 175, 107120. doi:10.1016/j.compositesb.2019.107120
- Khan, S. A., Kanwal, S., Rizwan, K., and Shahid, S. (2018a). Enhanced antimicrobial, antioxidant, *in vivo* antitumor and *in vitro* anticancer effects against breast cancer cell line by green synthesized un-doped SnO₂ and Co-doped SnO₂ nanoparticles from Clerodendrum inerme. *Microb. Pathog.* 125, 366–384. doi:10.1016/j.micpath.2018.09.041
- Khan, S. A., and Lee, C.-S. S. (2020). “Green biological synthesis of nanoparticles and their biomedical applications,” in *Springer science and business media B.V.*, 10, 247–280. doi:10.1007/978-3-030-44176-0_10
- Khan, S. A., Noreen, F., Kanwal, S., Iqbal, A., and Hussain, G. (2018b). Green synthesis of ZnO and Cu-doped ZnO nanoparticles from leaf extracts of abutilon

Funding

This study was supported by the Natural Science Foundation of Inner Mongolia Autonomous Region, China (2020MS08018), and the University Scientific Research Project of Inner Mongolia Autonomous Region, China (NJZY22134).

Acknowledgments

We would like to thank the Natural Science Foundation of Inner Mongolia Autonomous Region, China (2020MS08018), and the University Scientific Research Project of Inner Mongolia Autonomous Region, China (NJZY22134) for their support of this study.

Conflict of interest

The authors declare that the research was conducted in the absence of any commercial or financial relationships that could be construed as a potential conflict of interest.

Publisher's note

All claims expressed in this article are solely those of the authors and do not necessarily represent those of their affiliated organizations, or those of the publisher, the editors and the reviewers. Any product that may be evaluated in this article, or claim that may be made by its manufacturer, is not guaranteed or endorsed by the publisher.

indicum, clerodendrum infortunatum, clerodendrum inerme and investigation of their biological and photocatalytic activities. *Mater. Sci. Eng. C* 82, 46–59. doi:10.1016/j.msec.2017.08.071

Khan, S. A., Rizwan, K., Shahid, S., Noamaan, M. A., Rasheed, T., and Amjad, H. (2020b). Synthesis, DFT, computational exploration of chemical reactivity, molecular docking studies of novel formazan metal complexes and their biological applications. *Appl. Organomet. Chem.* 34, e5444. doi:10.1002/aoc.5444

Khan, S. A., Shahid, S., Ayaz, A., Alkahtani, J., Elshikh, M. S., and Riaz, T. (2021). Phytomolecules-coated NiO nanoparticles synthesis using abutilon indicum leaf extract: Antioxidant, antibacterial, and anticancer activities. *Int. J. Nanomedicine* 16, 1757–1773. doi:10.2147/IJN.S294012

Khan, S. A., Shahid, S., and Lee, C.-S. S. (2020a). Green synthesis of gold and silver nanoparticles using leaf extract of clerodendrum inerme; characterization, antimicrobial, and antioxidant activities. *Biomolecules* 10, 835. doi:10.3390/biom10060835

Khan, S. A., Shahid, S., Nazir, M., Kanwal, S., Zaman, S., Sarwar, M. N., et al. (2019b). Efficient template based synthesis of Ni nanorods by etching porous alumina for their enhanced photocatalytic activities against methyl red and methyl orange dyes. *J. Mol. Struct.* 1184, 316–323. doi:10.1016/j.molstruc.2019.02.038

Li, Z., Chen, J., Yang, J., Su, Y., Fan, X., Wu, Y., et al. (2015). β -Cyclodextrin enhanced triboelectrification for self-powered phenol detection and electrochemical degradation. *Energy Environ. Sci.* 8, 887–896. doi:10.1039/c4ee03596h

Liu, C., Kong, D., Hsu, P.-C., Yuan, H., Lee, H.-W., Liu, Y., et al. (2016). Rapid water disinfection using vertically aligned MoS₂ nanofilms and visible light. *Nat. Nanotechnol.* 11, 1098–1104. doi:10.1038/nnano.2016.138

Liu, J., Alvarez, J., and Kaifer, A. E. (2000). Metal nanoparticles with a knack for molecular recognition. *Adv. Mat.* 12, 1381–1383. doi:10.1002/1521-4095(200009)12:18<1381::aid-adma1381>3.0.co;2-u

Lu, H., Zhang, X., Khan, S. A., Li, W., and Wan, L. (2021). Biogenic synthesis of MnO₂ nanoparticles with leaf extract of viola betonicifolia for enhanced antioxidant, antimicrobial, cytotoxic, and biocompatible applications. *Front. Microbiol.* 2021, 761084. doi:10.3389/fmicb.2021.761084

Negishi, Y., Tsunoyama, H., Yanagimoto, Y., and Tsukuda, T. (2005). Subnanometer-sized gold clusters with dual molecular receptors: Synthesis and assembly in one-dimensional arrangements. *Chem. Lett.* 34, 1638–1639. doi:10.1246/cl.2005.1638

Sher, M., Khan, S. A., Shahid, S., Javed, M., Qamar, M. A., Chinnathambi, A., et al. (2021). Synthesis of novel ternary hybrid G-C₃N₄@Ag-ZnO nanocomposite with

Z-scheme enhanced solar light-driven methylene blue degradation and antibacterial activities. *J. Environ. Chem. Eng.* 9, 105366. doi:10.1016/j.jece.2021.105366

Siegel, R. L., Miller, K. D., and Jemal, A. (2020). Cancer statistics, 2020. *Ca. A Cancer J. Clin.* 70, 7–30. doi:10.3322/caac.21590

Wang, M., Fang, G., Liu, P., Zhou, D., Ma, C., Zhang, D., et al. (2016). Fe₃O₄@ β -CD nanocomposite as heterogeneous fenton-like catalyst for enhanced degradation of 4-chlorophenol (4-CP). *Appl. Catal. B Environ.* 188, 113–122. doi:10.1016/j.apcatb.2016.01.071

Wang, W., Li, G., Xia, D., An, T., Zhao, H., and Wong, P. K. (2017). Photocatalytic nanomaterials for solar-driven bacterial inactivation: Recent progress and challenges. *Environ. Sci. Nano* 4, 782–799. doi:10.1039/c7en00063d

Xu, Z., Feng, Q., Wang, M., Zhao, H., Lin, Y., and Zhou, S. (2020). Green biosynthesized silver nanoparticles with aqueous extracts of ginkgo biloba induce apoptosis via mitochondrial pathway in cervical cancer cells. *Front. Oncol.* 10, 575415. doi:10.3389/fonc.2020.575415

Yang, Y., Wang, C., Wang, N., Li, J., Zhu, Y., Zai, J., et al. (2022). Photogenerated reactive oxygen species and hyperthermia by Cu₃SnS₄ nanoflakes for advanced photocatalytic and photothermal antibacterial therapy. *J. Nanobiotechnology* 20, 195–219. doi:10.1186/s12951-022-01403-y

Yang, Z., Zhang, X., and Cui, J. (2014). Self-assembly of bioinspired catecholic cyclodextrin TiO₂ heterosupramolecule with high adsorption capacity and efficient visible-light photoactivity. *Appl. Catal. B Environ.* 148, 243–249. doi:10.1016/j.apcatb.2013.11.002

Zhang, X., Li, X., and Deng, N. (2012). Enhanced and selective degradation of pollutants over cyclodextrin/TiO₂ under visible light irradiation. *Ind. Eng. Chem. Res.* 51, 704–709. doi:10.1021/ie201694v

Zhang, X., Wu, F., and Deng, N. (2010). Degradation of paracetamol in self assembly β -cyclodextrin/TiO₂ suspension under visible irradiation. *Catal. Commun.* 11, 422–425. doi:10.1016/j.catcom.2009.11.013

Zhao, B., Wang, Y., Yao, X., Chen, D., Fan, M., Jin, Z., et al. (2021). Photocatalysis-mediated drug-free sustainable cancer therapy using nanocatalyst. *Nat. Commun.* 12, 1–11. doi:10.1038/s41467-021-21618-1

Zhu, H., Goswami, N., Yao, Q., Chen, T., Liu, Y., Xu, Q., et al. (2018). Cyclodextrin-gold nanocluster decorated TiO₂ enhances photocatalytic decomposition of organic pollutants. *J. Mat. Chem. A Mat.* 6, 1102–1108. doi:10.1039/C7TA09443D